Intercalation Mechanism and Interlayer Structure of Hexadecylamines in the Confined Space of Layered α-Zirconium Phosphates

Bongwoo Ha,[†] Kookheon Char,*[,†] and Hyun Sik Jeon[‡]

School of Chemical and Biological Engineering and Polymer Thin Films National Research Laboratory, Seoul National University, San 56-1, Shillim-dong, Kwanak-gu, Seoul 151-744, Korea, and Department of Petroleum and Chemical Engineering, New Mexico Institute of Mining & Technology, 801 Leroy Place, Socorro, New Mexico 87801

Received: September 29, 2005

Well-defined hexadecylamine (HDA) intercalated structures, either interdigitated layers, bilayers, or hybrid layers of both, in a confined space of highly functionalized layered α-zirconium phosphates (α-ZrPs) have been prepared based on the two-step intercalation mechanism and these distinct intercalated structures can serve as a model system to investigate the interactions of two monolayers whose amphiphilic tails are adjacent to each other. At the first intercalation step, the electrostatic interaction between HDAs and α-ZrP is dominant and results in an interdigitated layer structure (d_{001} = 3.0 nm) and the interdigitated layer is saturated at around Φ = 50%, where Φ is the weight fraction of intercalated HDAs in the intergallery of α-ZrP. For Φ higher than 50%, the bilayer structure (d_{001} = 4.3 nm) emerges due to further hydrophobic interaction between HDAs initially grafted to α-ZrP and unanchored HDAs and the relative fraction of the bilayer structure over the interdigitated layer increases with the increase in the intercalated amount of HDAs. The intriguing morphology of α-ZrP tactoids intercalated with HDAs in coexisting bilayers and interdigitated layers is observed by using microtomed TEM and the two-step intercalation has also been verified with TGA and FT-IR. Also, a structural transition from the bilayers to the interdigitated layers is monitored by using in situ synchrotron WAXS showing that the hydrophobically intercalated HDAs are selectively deintercalated at a relatively low decomposition temperature around 220 °C.

Introduction

Layered zirconium phosphates and phosphonates constitute a family of compounds that are quite attractive for material chemists.[1−3] The α-zirconium phosphate (α-$Zr(HPO_4)_2 \cdot H_2O$, α-ZrP) is considered as the archetype of the family. Clearfield et al.[4,5] first synthesized acid catalysts with a layered crystalline structure in the 1960s and thereafter there have been ample experimental studies on the use of α-ZrPs in molecular sieves, catalysts, ion and proton conductors, matrixes for chemical modification,[6−10] and as the inorganic component in polymer−inorganic hybrid materials.[11,12] Acidic functional groups (−POH) in the α-ZrP are in well-ordered array and the number of such functional groups is known to be quite high (i.e., cationic exchange capacity = 664 mmol/100 g, occupied area per charge site = 0.24 nm^2). Also, this huge number of functional groups is enough to afford bilayers within the α-ZrP interlayer because the cross-sectional area perpendicular to the chain axis of a single alkyl chain in the crystalline state is about 0.20 nm.[2,13−15] Accordingly, guest molecules with basic end-functional groups such as alkylamines (n-$C_nH_{2n+1}NH_2$)[16−18] and alkanol (n-$C_nH_{2n+1}OH$)[19,20] can readily be intercalated into the host of α-ZrPs by the acid−base reactions, which results in the formation of two monolayers on both sides of a α-ZrP intergallery.

Two monolayers whose alkyl tails face against each other find a broad array of applications such as biosensors,[21−23] colloid stability,[24,25] nanoencapsulation,[26−28] and protein immobilization.[29−31] An important issue in these self-assembled materials in confined geometry is to investigate interfacial structure between two monolayers, i.e., either interdigitation between the two monolayers (*interdigitated layers*) or discrete two monolayers (*bilayers*). For example, the interdigitation between long alkyl tails of monolayers of amphiphilic molecules has resulted in the formation of Langmuir−Blodgett films which can be used to fabricate stable multilayer films with three-dimensional arrays.[14,32,33] Also, the interfacial structure involving two monolayers has been investigated to determine the origin of the hysteresis during a loading−unloading cycle in adhesion experiments.[34−37] In addition, Ungar et al. observed the molecular interdigitation of a triple layer superlattice structure with a periodicity up to 50 nm in binary mixtures of long n-alkanes, where the interdigitated crystalline layers or phase formed can serve as an ideal model for studies such as the crystallization of polymers and the polymer chain folding.[15,38,39]

The purpose of this work is to explore the two-step intercalation mechanism for the preparation of well-defined crystalline films in either interdigitated layers or bilayers in the confined space of α-ZrP intergalleries. We have investigated the interlayer structures, whether in interdigitated layers, bilayers, or mixtures of both, for well-defined hexadecylamine (HDA) crystalline films in the confined geometry of α-zirconium phosphates. In addition, the HDA-intercalated α-ZrP hybrid system can be used as a model to study the structure and characteristics of two monolayers in the confined space of layered hybrid materials. The interlayer structure of HDA molecules confined in the α-ZrP intergalleries was characterized with wide-angle X-ray scattering (WAXS) and intriguing morphologies of α-ZrP tactoids consist-

[†] Seoul National University.
[‡] New Mexico Institute of Mining & Technology.

10.1021/jp055563h CCC: $30.25
Published on Web 12/01/2005

ing of bilayers and interdigitated layers of intercalated HDAs have also been observed with TEM. Also, the structural transition from bilayers to interdigitated layers was monitored with in situ synchrotron wide-angle X-ray scattering (WAXS).

Experimental Section

Inorganic α-zirconium phosphates (α-ZrPs) having a layered crystalline structure were synthesized according to the published procedures.[5] A 20-g sample of $ZrOCl_2 \cdot 8H_2O$ was dissolved in 100 mL of water and 34 g of 85% phosphoric acid was then added to this solution, resulting in the formation of a thick gelatinous product. The hydrofluoric acid (17 g, 172 mmol, 9 M) was then added to the gel while stirring until a clear solution was obtained. This reaction mixture was stirred at 80 °C for 7 days and water was added periodically to make up the lost volume. The precipitated materials as white powders were filtered and washed with plenty of water, and then dried in a vacuum oven at 100 °C for 72 h prior to use.

Hexadecylamine (HDA) was purchased from Aldrich and used as received. The HDA-intercalated α-ZrP materials used in this study were prepared via the following procedure. First, 0.1 g of α-ZrP was dispersed in a 50:50 mixture of H_2O and ethanol (500 mL) and the mixture was sonicated for about 10 min to obtain well-dispersed colloidal suspensions. Various amounts of HDA dissolved in ethanol were added dropwise to the colloidal suspensions containing α-ZrP powders. These mixtures were then stirred at 50 °C for about 24 h until HDAs were fully intercalated into the α-ZrP intergalleries. The resulting HDA-intercalated α-ZrP suspensions were filtered and subsequently washed with plenty of distilled water and ethanol solutions to remove HDA molecules not intercalated. The final products were dried in a vacuum oven at 100 °C for about 72 h.

Thermogravimetric analysis (TGA, TA Instruments) was employed to measure the amount of HDAs intercalated into the intergalleries of α-ZrP. The temperature for the TGA measurement was initially equilibrated at 100 °C for 10 min to remove residual moisture and the samples were heated at a rate of 10 °C /min up to 500 °C under nitrogen atmosphere. The differential scanning calorimetry (DSC) measurements on the HDAs intercalated into α-ZrP intergalleries were performed with a TA 2010 (TA Instruments) under nitrogen atmosphere. The temperature was initially maintained at −10 °C for 10 min and the intercalated α-ZrP samples were heated with subsequent cooling at a scanning rate of 10 °C/min up to 150 °C DSC curves for HDAs intercalated into α-ZrP intergalleries. The thermograms are recorded with first heating and subsequent cooling at a scanning rate of 10 °C/min from −10 °C to 150 °C. Fourier Transform infrared (FT-IR) spectroscopy measurements were carried out with a Bomem DA-8 instrument and all the samples in powder form were measured by using KBr pellets.

TEM was used to identify the layered morphology of HDA-intercalated α-ZrPs with different amount of HDAs. The powder samples were well dispersed in epoxy resin and epoxy/α-ZrP composites were cured at 60 °C for about 24 h for the TEM measurements. The electron transparent films of these epoxy/α-ZrP composites with nominal thicknesses of 80 to 100 nm were microtomed by using a diamond knife on a Leica Ultracut UCT and transferred onto Cu grids coated with carbon films. TEM measurements were performed on a JEOL JEM-2000EXII. Synchrotron WAXS measurements were performed at the 4C2 beam line in Pohang Light Source. The X-ray wavelength was 1.54 Å and the sample-to-detector distance was set at 20.5 cm.

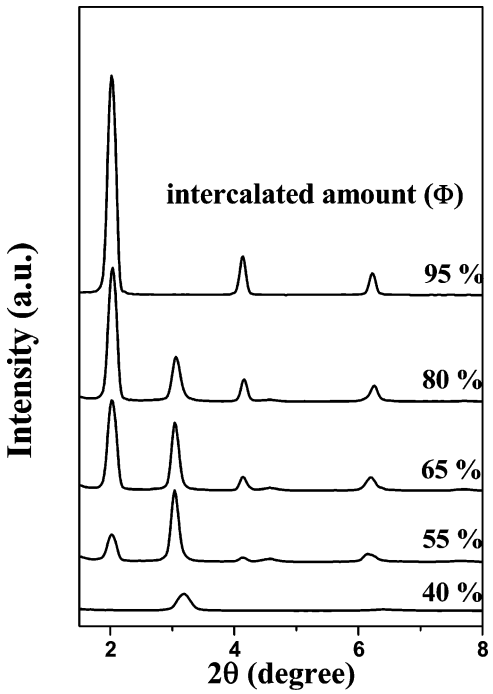

Figure 1. WAXS patterns of α-ZrPs as a function of the amount of intercalated HDAs (Φ = 40%, 55%, 65%, 80%, and 95%). The scattering traces of α-ZrPs intercalated with HDA at different Φ values are vertically shifted for clarity.

In situ scattering profiles were obtained from a HDA intercalated α-ZrP sample with 80% of full intercalation, verified by TGA, as a function of temperature ranging from 150 to 240 °C at a heating rate of 1 °C/min. Before the heating scan, all the samples were maintained at 150 °C for about 20 min.

Results and Discussion

Figure 1 shows the WAXS profiles for α-zirconium phosphate (α-ZrP) samples intercalated with hexadecylamine (HDA) as a function of the amount of intercalated HDAs (Φ = 40%, 55%, 65%, 80%, and 95%), where the intercalated HDA amount obtained from TGA measurements[40,41] is presented in terms of the relative extent of intercalation with respect to the theoretical full intercalation based on the number of HDA sites on the surface of α-ZrP layers. The WAXS profiles with different amounts of intercalated HDAs in the α-ZrPs are vertically shifted for clarity. At a low pillaring content (Φ = 40%), there is a single broad scattering peak at $2\theta = 3.2°$ ($d_{001} = 2.8$ nm) corresponding to the interdigitated layers of intercalated HDAs. With the increase in the intercalated HDA amount from 55% to 80% two distinct peaks coexist: one at a lower angle located at $2\theta = 2.05°$ ($d_{001} = 4.3$ nm) and the other at 2.95° ($d_{001} = 3$ nm). These two scattering peaks correspond to the bilayer and interdigitated layer structures of intercalated HDAs, respectively. It is quite interesting to note that the relative peak intensity for the interdigitated layer at $2\theta = 2.95°$ reaches its maximum at around Φ = 55% and the scattering intensity assigned for the interdigitated layers decreases with further increase in the pillaring content up to 80% and completely disappears at Φ = 95%. In contrast, the relative intensity assigned for the bilayers at $2\theta = 2.05°$ increases as the amount of intercalated HDAs is increased from 55% to 95%. Moreover, the *d* spacing value and the scattering intensity for the interdigitated layers at Φ = 40% are relatively smaller than those for Φ higher than 50%, indicating that the amount of intercalated HDAs at Φ = 40% is not sufficient to form well-ordered interdigitated layers.

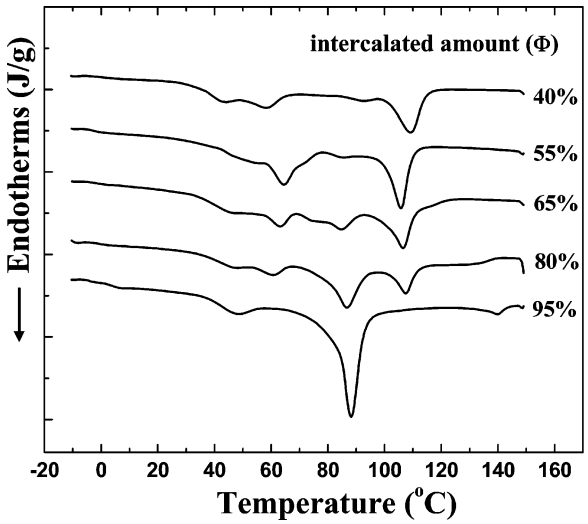

Figure 2. DSC curves for HDAs intercalated into α-ZrPs as a function of the amount of intercalated HDAs (Φ = 40%, 55%, 65%, 80%, and 95%). The DSC thermograms were recorded at the first heating scan from −10 to 150 °C with a heating rate of 10 °C/min and are also vertically shifted for clarity.

To examine the effect of the amount of intercalated HDAs on the formation of crystalline HDA films in confined geometry, we performed DSC experiments for different samples with 40% ≤ Φ ≤ 95% and the results are shown in Figure 2. For Φ = 95%, it is clear that a large endothermic peak corresponding to the melting of intercalated HDAs is shown at T = 88 °C, indicating the formation of thin crystalline films in the bilayers.[20,42] With the decrease in the pillaring contents from 95% to 40%, two new transitional peaks emerge at T = ∼62 and ∼107 °C. It is also noted that the value of the enthalpic change at T = 107 °C is always higher than the value at T = 62 °C. It has been reported that intercalated HDAs in the confined space of layered bentonites exhibit multiple melting temperatures as the interlayer structure is varied.[43] Since the transition peaks at T = 62 and 107 °C are also related to the melting transition of intercalated HDAs, the melting transitions suggest that thin crystalline films are formed at Φ = 50% due to the chain interdigitation between the two monolayers.[37]

Figure 3 shows the molecular structure of thin crystalline films formed either in bilayers or in interdigitated layers of HDAs inside α-ZrPs. We take simple geometric considerations on the bilayers (Figure 3a) and the interdigitated layers (Figure 3b) to estimate the tilted angles of HDA molecules intercalated into the α-ZrP intergalleries. As shown in Figure 3a the thickness of a single HDA layer in the bilayer structure is estimated to be 1.83 nm [(4.3 − 0.65)/2] based on the bilayer model by measuring the d spacing of the bilayer (d_{001} = 4.3 nm) as well as the thickness of a single clay sheet (l = 0.65 nm). If an alkyl chain in a single HDA layer is assumed to take all-trans zigzag conformation, equivalent to the asymmetric CH_2 stretching band at ∼2918 cm^{-1} and the symmetric CH_2 stretching band at ∼2850 cm^{-1} from FT-IR,[44] its average chain end-to-end distance is approximately 2.05 nm. The tilt angle of HDAs in the α-ZrP layer is thus estimated to be about 25° [90° − $\sin^{-1}$ (1.83/2.05)]. However, it is not easy to estimate the tilt angle for the interdigitated layers since there is room for free space between the end of tethered HDA tails emanating from the other α-ZrP surface and the α-ZrP surface (see Figure 3b). It has been reported that the tilt angle in crystalline monolayers is quite sensitive to the distance between neighboring adsorbed molecules and the average size of headgroups of amphiphilic molecules is eventually related to the distance between two neighboring adsorbed molecules.[13,14] The mean distance between two neighboring HDAs for both bilayers and interdigitated layers is assumed to be similar because they both occupy the same area on the surface of the α-ZrP layer, i.e., ∼0.24 nm^2 per single HDA molecule. We thus assume that the tilt angle for the interdigitated layers is similar to that for the bilayers.

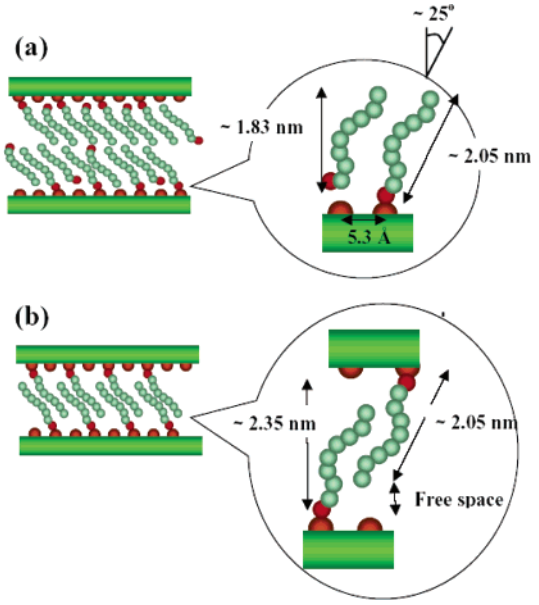

Figure 3. Schematics on the molecular structures of crystalline thin HDA films in bilayers (a) and in interdigitated layers (b) in α-ZrP intergalleries. The thicknesses of a single HDA layer in the bilayers (∼1.83 nm) and an interdigitated layer (∼2.35 nm) are estimated from the d spacing values measured from WAXS (4.3 and 3 nm, respectively) and the layer thickness of a single α-ZrP sheet (=0.65 nm).

Figure 4 shows typical microtomed bright-field TEM images of intercalated structures for the HDA intercalated into α-ZrP at three different intercalated amounts: (a) Φ = 95%, (b) Φ = 55%, and (c) Φ = 65%. The three different images clearly show the bilayers (Figure 4a), the interdigitated layers (Figure 4b), and the coexistence of both bilayers and interdigitated layers (Figure 4c). The period distances obtained from the TEM images are in excellent agreement with the numbers deduced from the WAXS measurements (see Figure 1). It is evident that the tactoids of intercalated α-ZrPs show well-ordered layered structure. The individual α-ZrP sheets are shown as dark lines in the micrographs, from which the thicknesses between individual sheets (i.e., d spacing) normal to the prismatic {110} or {010} surface can be estimated. In Figure 4a, a majority of interlayer distance between the dark lines within the tactoids is found to be 4.3 nm, corresponding to the d spacing of the bilayer structure obtained from the scattering measurements. In Figure 4b, the interlayer distance between the two individual sheets within the tactoids is dominantly 3 nm, again corresponding to the d spacing of the interdigitated layer structure. Figure 4c, however, shows a quite intriguing tactoid structure consisting of two different interlayer distances, 4.3 and 3 nm, leading to the coexistence of both bilayers and interdigitated layers within a tactoid. In addition to the coexistence of both bilayers and interdigitated layers within a α-ZrP tactoid, we also found that there are regions of the tactoids in which only bilayers or interdigitated layers are observed for Φ = 65%.

To measure the amount of HDAs intercalated into the α-ZrP, we performed the TGA experiments for all the α-ZrP samples studied here. Figure 5a shows the weight losses of the α-ZrP samples as a function of temperature scanned from 100 to 500 °C at a heating rate of 10 °C/min. Figure 5b also shows the

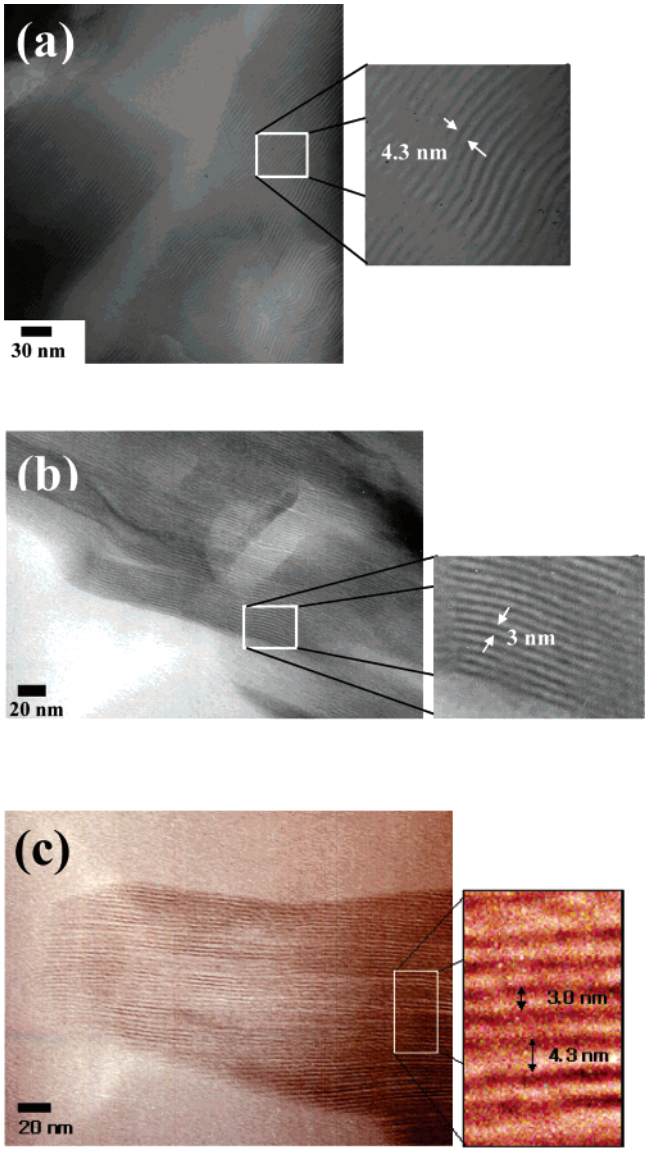

Figure 4. TEM images of α-ZrPs intercalated with HDA at (a) Φ = 95%, (b) Φ = 55%, and (c) Φ = 65%. The boxed region in each TEM image is also magnified on the right-hand side. The α-ZrP sheets are shown as darker lines representing the thickness between individual clay sheets normal to the prismatic {110} or {010} surface. All the scale bars in TEM images are 20 nm.

derivatives of the weight losses based on the TGA curves for samples with different intercalated amount, providing peak temperatures at which the maximum weight losses occur. Independent experiment verifies that the host component, α-ZrP, does not decompose in the temperature range set for monitoring the degradation of intercalated HDAs. It is surprising to note that there are two distinct temperatures corresponding to the weight loss arising from the decomposition of intercalated HDAs. For Φ higher than 55%, the weight loss of intercalated HDAs at a peak temperature residing between 220 and 250 °C starts to emerge in addition to the degradation of HDAs at a higher peak temperature of 320 °C. It is also interesting to note that the relative portion of the degradation of intercalated HDAs at a lower temperature around 230 °C increases as the intercalation amount (Φ) is increased. The degradation of intercalated HDAs at Φ lower than 55% dominantly occurs at the high degradation temperature at 320 °C.

The two-step weight loss behavior observed in the TGA/DTG curves, shown in Figure 5, is believed to originate from different

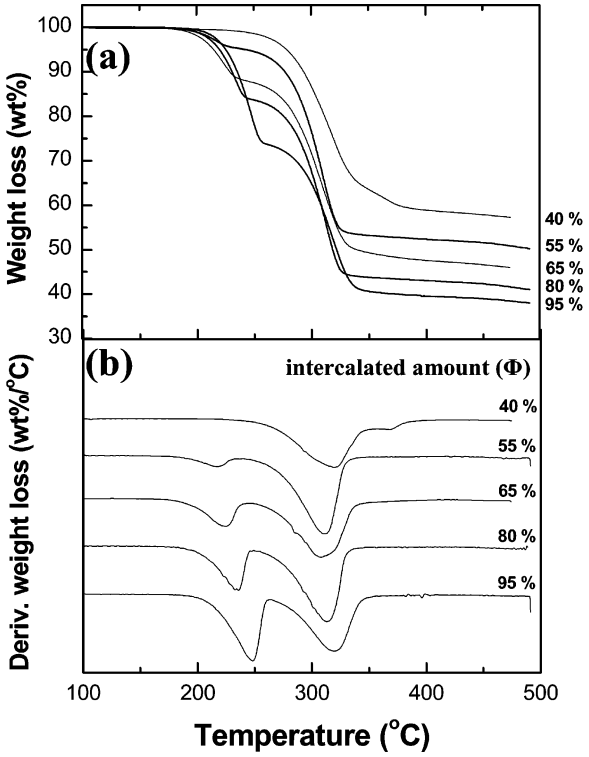

Figure 5. (a) TGA curves for α-ZrPs intercalated with different amounts of HDA as a function of temperature. The α-ZrP samples intercalated with HDA were initially maintained at 100 °C for about 10 min and then heated to 500 °C at a rate of 10 °C/min. The derivative of the weight loss for each TGA curve is also obtained and shown in part b. Each curve in part b is vertically shifted for clarity.

interactions among HDAs intercalated into the α-ZrPs, i.e., electrostatic and hydrophobic interactions. Since most of intercalated HDAs are strongly bound to the α-ZrP surface with the electrostatic interaction for Φ = 40%, the deintercalation or thermal decomposition of intercalated HDAs occurs at a relatively high temperature of 320 °C. This explains the reason the degradation of HDAs at 320 °C is dominant up to Φ ≈ 55%. Since further intercalation of HDAs into α-ZrP intergalleries is possible through the hydrophobic interaction of incoming HDAs with preanchored HDAs, we believe that the degradation at a lower temperature around 230 °C is due to the weaker interaction among intercalated HDAs. It is also reasonable to assume that the intercalation amount (Φ) increases due to these weaker interactions among HDAs in α-ZrP.

To further verify the two-step intercalation process, we examined the characteristic vibrations of end-functional amines of the intercalated HDAs from FT-IR measurements on α-ZrP/HDA hybrid samples. Figure 6 shows the FT-IR spectra at different amounts of intercalated HDAs. It is evident that the NH_2 scissoring band assigned at ∼1550 cm^{-1} is split into two bands for Φ higher than 65%. This is because the amines anchored directly onto the α-ZrP surface are in a different energy level when compared with the vibrational energy level of unanchored *free* amines. For Φ lower than 65%, there is only a single band of $\delta(NH_2)$ at ∼1550 cm^{-1}, corresponding to the amines in direct contact with the α-ZrP surface. In contrast, another $\delta(NH_2)$ peak emerges in addition to the band at 1550 cm^{-1} for Φ higher than 65%. A new band at a frequency of ∼1600 cm^{-1} is related to unanchored *free* amines of HDAs intercalated due to the secondary hydrophobic interactions, and the relative intensity of the new band increases with the increase in Φ up to 95%. Although the HDAs deintercalated (or decomposed) at a relatively low temperature of ∼230 °C are

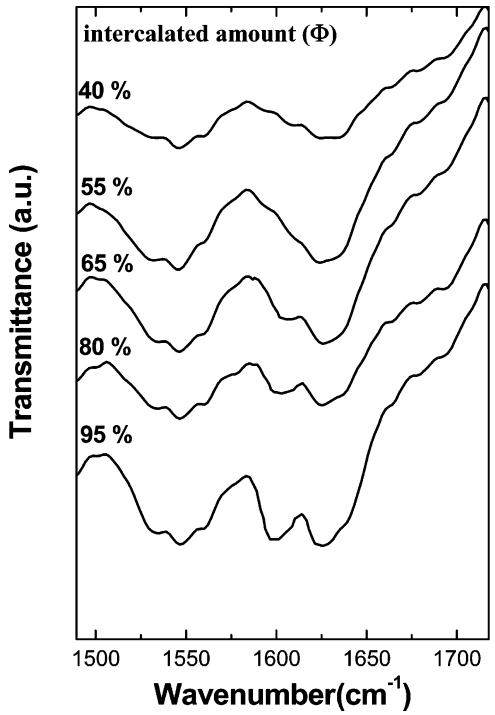

Figure 6. FT-IR spectra of HDAs intercalated into the α-ZrP intergalleries as a function of the amount of intercalated HDAs (Φ = 40%, 55%, 65%, 80%, and 95%) in the frequency region representing the NH_2 scissoring band, $\delta(NH_2)$. Each curve in the FT-IR data is shifted vertically for clarity.

clearly observed for Φ = 55% (see Figure 5), the $\delta(NH_2)$ band at a frequency of 1600 cm^{-1} is not found (see Figure 6) because we presume that the amount of unanchored *free* amines is too small to manifest itself in the FT-IR data.

Figure 7 represents a schematic on the intercalation mechanism and the interlayer structure of HDAs intercalated into the α-ZrPs based on the experimental data gathered so far. There are two possible structures in the HDA intercalated system: the interdigitated layer structure (shown in the upper right corner) and the bilayer structure (shown in the lower right corner). The intercalation mechanism could be described with a model of the diffusion of small HDA molecules into the layered space with a fixed dimension. This intercalation mechanism is also quite interesting since the diffusion of HDA molecules into the interlayer space of α-ZrP is usually hindered by the narrow basal spacing of layered α-ZrPs. The basal spacing (d_{001} = 0.76 nm) of dried α-ZrP layers is relatively much smaller than the size of a HDA molecule (~2.05 nm in chain length with all-trans zigzag conformation). It is known that the hindered diffusion of molecules in confined space can be overcome by the enthalpic interactions of the terminal amine groups of HDA molecules with acidic −POH groups on the surface of α-ZrPs and the van der Waals interactions between the adjacent molecules, where the HDA molecules can penetrate into the narrow gallery spacing and then expand the basal spacing. Once the thermodynamic barrier for intercalation is removed, free HDA molecules in bulk solution can easily diffuse into the expanded spacing.

To demonstrate two well-defined intercalated structures, interdigitated layers and bilayers, of HDAs in the confined layered geometry of α-ZrPs, a two-step intercalation mechanism is postulated and schematically shown in Figure 7. First, the electrostatic interaction between negatively charged α-ZrP and positively charged HDAs is dominant during the initial intercalation step. At this intercalation step, the steric hindrance among intercalated HDA molecules also significantly affects the HDA intercalation and its intercalated structure. In other words, only a single HDA molecule is, on average, preferentially tethered onto every other charge site located on the surface of the α-ZrP layer because the hydrodynamic diameter of a HDA molecule in ethanol/H_2O mixture is quite a bit larger than the distance between average charge sites (~0.53 nm) of α-ZrP. This type of enthalpy-driven intercalation process is thus saturated at about 50% of full HDA intercalation amounts (Φ = 50%) and provides well-ordered monolayers of HDA molecules tethered onto alternate charge sites of α-ZrPs. After the initial intercalation process, thin crystalline HDA films within the α-ZrP intergalleries are obtained due to the minimization of the surface free energy of intercalated HDA molecules during evaporation and annealing processes. However, for Φ = 50%, the amount of HDAs intercalated into the intergalleries of α-ZrPs is not sufficient to form two discrete crystalline monolayers due to the low packing density of HDAs in the intergallery. In other words, the mean distance between two neighboring molecules for Φ = 50% is about 1.06 nm (i.e., 2 × 0.53 nm (average distance between charge sites on α-ZrP)), which is not close enough to form crystalline HDA films. Consequently, the interdigitation between the two HDA monolayers originating from each α-ZrP sheet occurs in order to minimize the surface free energy, and thin crystalline films with well-ordered interdigitated layers are formed and schematically described in the upper right corner of Figure 7.

The first enthalpic-driven intercalation process mainly due to the electrostatic interaction provides the saturation of HDAs with Φ = 50%, resulting in the interdigitated structure of intercalated HDA chains within the α-ZrP intergalleries. In contrast, in the second step of the intercalation process at Φ higher than 50%, it is expected that the long alkyl chains of the intercalated HDAs have rather preferred hydrophobic interaction with those HDAs preanchored onto the surface of a α-ZrP layer over the direct electrostatic interaction with the α-ZrP surface and thus fill vacant sites between the preanchored HDAs. Since the HDA monolayers formed between the α-ZrP layers have a high packing density due to the highly intercalated HDA molecules during the second intercalation step, the formation of the interdigitated layer between two HDA monolayers is not necessary during the crystalline packing process of the two monolayers. As a result, the two discrete crystalline monolayers consisting of tilted hydrocarbon chains form bilayers after evaporation and annealing steps. Consequently, we conclude that the structural transition from interdigitated layers to bilayers during the intercalation with HDAs occurs at Φ around 50% when the second-step intercalation through the secondary hydrophobic interaction comes into play.

Based on the two-step deintercalation demonstrated in Figure 5, we can postulate that a structural change or a transition from the bilayers to the interdigitated layers would be possible if the hydrophobically intercalated HDAs in the α-ZrP are first allowed to deintercalate (or decompose) at the low annealing temperature around ~230 °C. To confirm such a postulation on the structural change during the heating process, we performed in situ synchrotron wide-angle X-ray scattering (WAXS) experiments during a heating scan from 150 to 240 °C at a rate of 1 °C /min and the results are shown in Figure 8. Figure 8a shows the WAXS profiles as a function of temperature for a sample with Φ = 80%, and the change of d spacings ($=2\pi/q$) and the relative scattered intensities $\Omega_i(T)$, based on the three scattering peaks assigned as P_1 (bilayers), P_2 (intermediate layers), and P_3 (interdigitated layers)), are also presented in

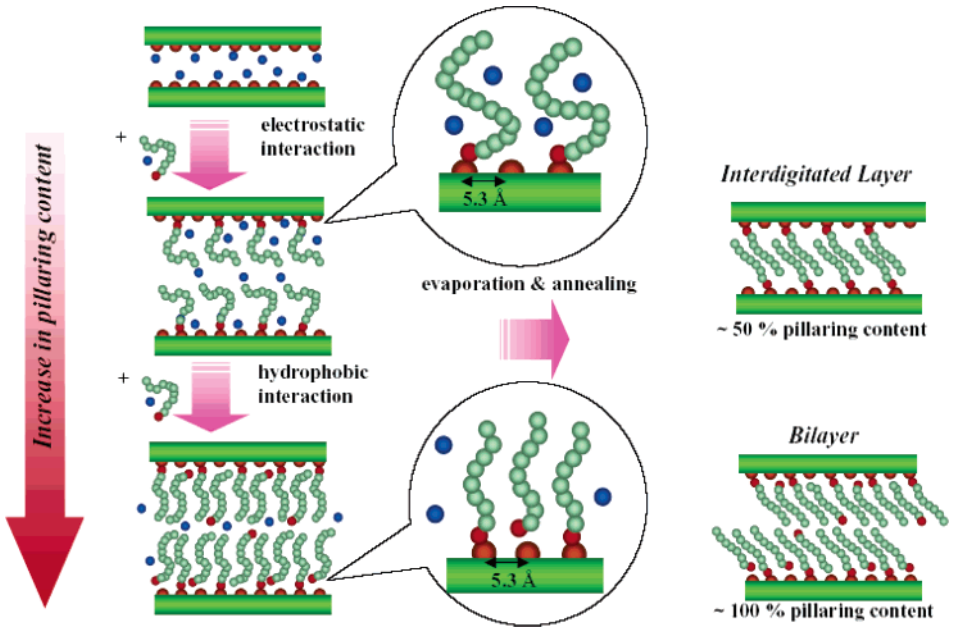

Figure 7. A schematic showing the two-step mechanism of HDA intercalation into α-ZrP intergalleries. The mean distance between charge sites (−POH) on the surface of the α-ZrP layer is about 5.3 Å.

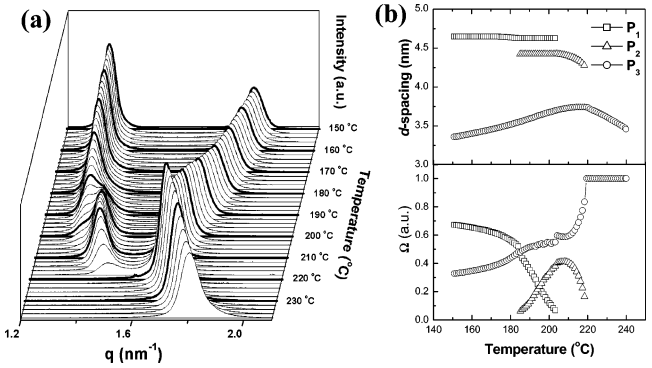

Figure 8. (a) Temperature-programmed WAXS profiles of α-ZrPs intercalated with HDA at $\Phi = 80\%$ as a function of temperature. The intercalated α-ZrP samples were initially conditioned at 150 °C for about 10 min and then heated at a rate of 1 °C /min up to 240 °C. (b) The *d* spacing ($=2\pi/q_{max}$) and the relative fractions ($\Omega_i(T) \equiv I_i(T)/\sum I_i(T)$) of contributions from three different scattering peaks, P_1 (bilayers), P_2 (intermediate layers), and P_3 (interdigitated layers), as a function of temperature.

Figure 8b. To gain details on the change of the relative population of scattering peaks (P_1, P_2, and P_3) as a function of the temperature, the relative scattered intensity of a given scattering peak *i*, $\Omega_i(T)$, defined as $\Omega_i(T) \equiv I_i(T)/\sum I_i(T)$ at temperature *T*, is introduced where $I_i(T)$ is the maximum scattering intensity of a peak *i* at a given temperature of *T*. At a low temperature around 150 °C, only two scattering peaks denoted as P_1 and P_3 with the *d* spacing values of 4.7 and 3.3 nm, respectively, exist. Based on our previous WAXS results for the sample with $\Phi = 80\%$, the P_1 and P_3 scattering peaks are assigned as bilayers and interdigitated layers of HDAs in α-ZrP, respectively. It is, however, noted that the *d* spacing values of bilayers and interdigitated layers given in Figure 8b are slightly higher than the values obtained from the WAXS measurements measured at room temperature (see Figure 1). It is generally known that the molecular volume occupied by intercalated HDAs in the confined space of α-ZrP intergallery increases as temperature is raised and this entropic penalty due to the thermal expansion of intercalated HDAs can be overcome by the expansion of the basal spacing of α-ZrPs.[42] When temperature is increased from 150 to 185 °C, the coexistence of both bilayers (P_1) and interdigitated layers (P_3) prevails. It is interesting to observe that at around $T = 185$ °C, the scattering intensity assigned to the bilayers (P_1) starts to decrease and, at the same time, a new intermediate peak (P_2) with a *d* spacing value of 4.3 nm emerges up to $T = 205$ °C while the scattering peak for the interdigitated layers (P_3) remains almost constant. The bilayer peak (P_1) completely disappears at $T = 205$ °C and the new peak denoted as P_2, which seems to evolve from the bilayer peak above 185 °C, goes through the maximum at $T = 205$ °C and again disappears at $T = 220$ °C. Above 220 °C there exists a single scattering peak assigned to the interdigitated layers (P_3). Consequently, these in situ scattering experiments confirm that the structural change from bilayers to interdigitated layers occurs at temperatures above 220 °C, which is in good agreement with the TGA measurements given in Figure 5. The combined TGA and temperature-resolved WAXS experiments represent that this type of the structural transition is due to the selective deintercalation of HDAs associated within the α-ZrP intergalleries through the relatively weak, hydrophobic interactions.

Conclusions

We have demonstrated for the first time that the two-step intercalation mechanism can induce well-defined intercalated structures of hexadecylamines (HDAs), either in bilayers or in interdigitated layers, in the confined space of highly functionalized layered α-zirconium phosphate (α-ZrP) intergalleries. At the initial intercalation process, the electrostatic interactions between HDAs and the surface charge of α-ZrPs are dominant and result in the formation of interdigitated layers and these interdigitated layers are found to reach the maximum at $\Phi \sim 50\%$, where Φ is the weight fraction of intercalated HDAs in the intergalleries of α-ZrP. For Φ above 50%, bilayer structures start to emerge due to the secondary hydrophobic interactions between HDAs preanchored onto α-ZrP surfaces and unanchored HDAs and the relative amount of the bilayers over the interdigitated layers increases as the amount of intercalated HDAs increases. Bilayers, interdigitated layers, or the mixtures of both of the HDAs intercalated into α-ZrP intergalleries are

confirmed with WAXS and TEM. The clue for the two-step intercalation is obtained by the TGA measurements showing two distinct decomposition temperatures at 230 and 320 °C corresponding to the weight losses arising from two different types of intercalated HDAs and this two-step intercalation mechanism is again verified by FT-IR spectra with a new NH_2 scissoring band at 1600 cm^{-1} related to *unanchored* free amines emerging on top of the anchored amines assigned at 1550 cm^{-1} above $\Phi = 50\%$. Also, temperature-resolved WAXS experiments confirm that a structural transition from bilayers to interdigitated layers is due to the selective deintercalation of HDAs related to the secondary hydrophobic interactions at a relatively low temperature of 220 °C.

Acknowledgment. This work was financially supported by the National Research Laboratory Program (Grant M1-0104-00-0191) and by the Ministry of Education through the Brain Korea 21 Program at Seoul National University. X-ray experiments performed at Pohang Light Source were supported by the Ministry of Science and Technology. We are also very grateful to Dr. Jinhan Cho for helpful discussions and to Mr. Daewon Lee for his assistance in X-ray experiments.

References and Notes

(1) Alberti, G.; Casciola, M.; Costantino, U.; Vivani, R. *Adv. Mater.* **1996**, *8*, 291.
(2) Clearfield, A.; Costantino, U. Layered Metal Phosphates and their Intercalation Chemistry. In *Comprehensive Supramolecular Chemistry*; Alberti, G., Bein, T., volume Eds.; Pergamon: New York, 1996; Vol. 7, p 107.
(3) Chearfield, A. Metal Phosphonate Chemistry. In *Progress in Inorganic Chemistry*; Karlin, K. D., Ed.; Wiley & Sons: New York, 1997; Vol. 47, pp 371−510.
(4) Clearfield, A.; Stynes. J. A. *J. Inorg. Nucl. Chem.* **1964**, *26*, 117.
(5) Alberti, G.; Torracca, E. *J. Inorg. Nucl. Chem.* **1968**, *30*, 317.
(6) *Inorganic Ion Exchange Materials*; Clearfield, A., Ed.; CRC Press: Boca Raton, FL, 1982.
(7) Aberti, G.; Costantino, U. In *Intercalation Chemistry*; Whittinghan, M. S., Jachbson, A. J., Eds.; Academic Press: New York, 1982.
(8) Alberti, G. In *Recent Developments in Ion Exchange*; Williams, P. A., Hudson, M. J., Eds.; Elsevier Applied Science: London, UK, 1987.
(9) Clearfield, A. In *Design of New Materials*; Plenum Press: New York, 1987.
(10) Alberti, G.; Costantino, U. In *Inclusion Compounds. Inorganic and Physical Aspects of Inclusion*; Atwood, J. L., Davis, J. E. D., MacNicol, D. D., Eds.; Oxford University Press: Oxford, UK, 1991; Vol. 5.
(11) Kim, H.-N.; Keller, S. W.; Mallouk, T. E.; Schmitt, J.; Decher, G. *Chem. Mater.* **1997**, *9*, 1414.
(12) Sue, H.-J.; Gam, K. T.; Bestaoui, N.; Spurr, N.; Clearfield, A. *Chem. Mater.* **2004**, *16*, 242.
(13) Kaganer, V. M.; Möhwald, H.; Dutta, P. *Rev. Mod. Phys.* **1999**, *71*, 779.
(14) Kuzmenko, I.; Rapaport, H.; Kjaer, K.; Als-Nielsen, J.; Weissbuch, I.; Lahav, M.; Leiserowitz, L. *Chem. Rev.* **2001**, *101*, 1659.
(15) Ungar, G.; Zeng, X. B. *Chem. Rev.* **2001**, *101*, 4157.
(16) Clearfield, A.; Tindwa, R. M. *J. Inorg. Nucl. Chem.* **1979**, *41*, 871.
(17) Gupta, J. P.; Nowell, D. V. *J. Chem. Soc., Dalton Trans.* **1979**, 1178.
(18) Alberti, G.; Costantino, U. *J. Mol. Catal.* **1984**, *27*, 235.
(19) Costantino, U. *J. Chem. Soc., Dalton Trans.* **1979**, 402.
(20) Costantino, U.; Vivani, R.; Zima, V.; Beneš, L.; Melánová, K. *Langmuir* **2002**, *18*, 1211.
(21) Tender, L. M.; Worley, R. L.; Fan, H.; Lopez, G. P. *Langmuir* **1996**, *12*, 5515.
(22) Peng, Z.; Tang, J.; Han, X.; Wang, E.; Dong, S. *Langmuir* **2002**, *18*, 4834.
(23) Glidle, A.; Yasukawa, T.; Hadyoon, C. S.; Anicet, N.; Matsue, T.; Nomura, M.; Cooper, J. M. *Anal. Chem.* **2003**, *75*, 2559.
(24) Swami, A.; Kumar, A.; Sastry, M. *Langmuir* **2003**, *19*, 1168.
(25) Fan, H.; Yang, Kai; Boye, D. M.; Sigmon, T.; Malloy, K. J.; Xu, H.; López, G. P.; Brinker, C. J. *Science* **2004**, *304*, 567.
(26) Bu, W.; Li, H.; Li, W.; Wu, L.; Zhai, C.; Wu, Y. *J. Phys. Chem. B* **2004**, *108*, 12776.
(27) Wang, Z. L.; Harfenist, S. A.; Whetten, R. L.; Bentley, J.; Evans, N. D. *J. Phys. Chem. B* **1998**, *102*, 3068.
(28) Kisak, E. T.; Coldren, B.; Zasadzinski, J. A. *Langmuir* **2002**, *18*, 284.
(29) Kumar, C. V.; McLendon, G. L. *Chem. Mater.* **1997**, *9*, 863.
(30) Kumar, C. V.; Chaudhari, A. *J. Am. Chem. Soc.* **2000**, *122*, 830.
(31) Chaudhari, A.; Thota, J.; Kumar, C. V. *Microporous Mesoporous Mater.* **2004**, *75*, 281.
(32) Kuzmenko, I.; Buller, R.; Bouwman, W. G.; Kjær, K.; Als-Nielsen, J.; Lahav, M.; Leiserowitz, L. *Science* **1996**, *274*, 2046.
(33) Kuzmenko, I.; Kindermann, M.; Kjaer, K.; Howes, P. B.; Als-Nielsen, J.; Granek, R.; v. Kiedrowski, G.; Leiserowitz, L.; Lahav, M. *J. Am. Chem. Soc.* **2001**, *123*, 3771.
(34) Israelachvili, J. N. *Vac. Sci. Technol. A* **1992**, *10*, 2961.
(35) Yoshizawa, H.; Chen, Y.-L.; Israelachvili, J. N. *J. Phys. Chem.* **1993**, *97*, 4128.
(36) Chaudhury, M. K.; Owen, M. J. *J. Phys. Chem.* **1993**, *97*, 5722.
(37) Karaborni, S. *Phys. Rev. Lett.* **1994**, *73*, 1668.
(38) Zeng, X. B.; Ungar, G. *Phys. Rev. Lett.* **2001**, *86*, 4875.
(39) Zeng, X. B.; Ungar, G. *Macromolecules* **2003**, *36*, 4686.
(40) Vaia, R. A.; Teukolsky, R. K.; Giannelis, E. P. *Chem. Mater.* **1994**, *6*, 1017.
(41) Lan, T.; Pinnavaia, T. J. *Chem. Mater.* **1994**, *6*, 2216.
(42) Barman, S.; Venkataraman, N. V.; Vasudevan, S.; Seshadri, R. *J. Phys. Chem. B.* **2003**, *107*, 1875.
(43) Li, Y.; Ishida, H. *Chem. Mater.* **2002**, *14*, 1398.
(44) The intensities of the bands at 2918 and 2850 cm^{-1}, attributed to CH_2 asymmetric and symmetric stretching vibrations, are found to increase with the increased amount of intercalated HDAs while the frequency shift of these bands is not observed for Φ between 40% and 95%.